Electronic Supplementary Material (ESI) for Journal of Materials Chemistry C.

Electronic Supplementary Information for

Interface Engineering Strategies towards $Cs_2AgBiBr_6$ Single-Crystalline Photodetectors with Good Ohmic Contact Behaviours

*Yangyang Dang, Guoqing Tong, Wentao Song, Zonghao Liu, Longbin Qiu, Luis K. Ono and Yabing Qi**

Energy Materials and Surface Sciences Unit (EMSSU), Okinawa Institute of Science and Technology Graduate University (OIST), 1919-1 Tancha, Onna-son, Kunigami-gun, Okinawa 904-0495, Japan
*Corresponding author: Yabing Qi, E-Mail: Yabing.Qi@OIST.jp

Experimental Section

Fig. S1. Photos of $Cs_2AgBiBr_6$ single crystals with and without MABr as flux.

Fig. S2. Crystal structures of $Cs_2AgBiBr_6$ single crystals at 293 and 100 K.

Fig. S3. Core level XPS spectra for (a) wide scan of $Cs_2AgBiBr_6$ single crystal, (b) N 1s, (c) Cs 3d, (d) Ag 3d, (e) Bi 4f and (f) Br 3d, fitted with peaks having a 70% Gaussian and 30% Lorentzian peak shape after applying background subtraction with Shirley function.

Fig. S4. Photos of high quality $Cs_2AgBiBr_6$ single crystals by using abrasive paper and then silk cloth.

Fig. S5. SCLC measurement of $Cs_2AgBiBr_6$ single crystal. (a) SCLC curve of $Cs_2AgBiBr_6$ single crystal; (b) Schematic illustration of SCLC based on $Cs_2AgBiBr_6$ single crystals.

Fig. S6. PL decay lifetime of $Cs_2AgBiBr_6$ single crystals, using biexponential fitting.

Fig. S7. (**a-d**) Photodetector data (I-V and I-time curves) of $Cs_2AgBiBr_6$ single crystal based on Au electrodes under different wavelength at room temperature when measured in air with a relative humidity of 20 % and under vacuum conditions (P = 3x10^{-7} Torr); (**e-h**) Photodetector data (I-V and I-time curves) of $Cs_2AgBiBr_6$ single crystal based on Al electrodes under different wavelength at room temperature when measured in air with a relative humidity of 20% and under vacuum conditions (P = 3x10^{-7} Torr).

Fig. S8. Energy band diagrams of the $Cs_2AgBiBr_6$ single-crystalline devices using different electrodes not in contact and in contact in the dark condition. Energy band diagrams of the $Cs_2AgBiBr_6$ single-crystalline devices using Ag electrodes not in contact (**a**) and in contact (**b**) in the dark; Energy band diagrams of the $Cs_2AgBiBr_6$ single-crystalline devices using Au electrodes not in contact (**c**) and in contact (**d**) in the dark.

Fig. S9. Response time and decay time of $Cs_2AgBiBr_6$ single-crystalline photodetectors.

Fig. S10. Stability of $Cs_2AgBiBr_6$ single-crystalline photodetectors in air and vacuum atmosphere at room temperature.

Fig. S11. (**a, c, e**) Photodetector data (I-V and I-time curves) of $Cs_2AgBiBr_6$ single crystal based on Ag electrodes at room temperature (293 K); (**b, d, f**) Photodetector data (I-V and I-time curves) of $Cs_2AgBiBr_6$ single crystal based on Ag electrodes at low temperature (100K). All the measurements were performed in under vacuum conditions (P = $3x10^{-7}$ Torr).

Table S1. Crystal data and structure refinements for $Cs_2AgBiBr_6$ at 293 and 100 K.

Table S2. Device parameters for $Cs_2AgBiBr_6$ single-crystalline photodetectors using Ag electrodes at different condition.

Table S3. Comparison of perovskite single crystal photodetectors in this work and previous reports operated in ambient air condition.

Experimental Section

Single-crystal X-ray diffraction and Powder X-ray diffraction studies: A suitable crystal $Cs_2AgBiBr_6$was selected and fixed on a '*Bruker APEX-II CCD*' diffractometer with the graphite-monochromatized Mo-Kα radiation, λ = 0.71073 Å. The crystal was kept at 293 and 100.0 K during data collection. Using *Olex2*,[1] and the structure was solved with the *XS*[2] structure solution program using *Direct Methods* and refined with the *XL*[2] refinement package using *Least Squares minimization*. X-ray powder diffraction (XRD) pattern of polycrystalline material was collected using a Bruker-AXS D8 Advance Muti-purpose X-ray diffractometer with $CuK\alpha_1$ radiation (λ = 1.54186 Å) in the range of 10-80^o (2θ).

UV-vis-NIR diffuse reflectance spectra measurements: UV-vis-NIR diffuse reflectance spectroscopy was carried out using a Varian Cary 5000 spectrophotometer equipped with an integrating sphere over the spectral range 200-900 nm. $Cs_2AgBiBr_6$ single crystals were dried and grinded into single-crystalline powders. A $BaSO_4$ plate was used as the standard (100% reflectance). The absorption spectrum was calculated from the reflectance spectrum using the Kubelka-Munk function: $\alpha/S= (1-R)^2/(2R)$,[3] where α is the absorption coefficient, *S* is the scattering coefficient, and R is the reflectance.

XPS and UPS measurements and analyses: Single-crystalline samples were cleaved inside an Ar glovebox and then extracted using a sample transporter that protects against air exposure. The sample transporter is connected to the ultra-high vacuum chamber and then transferred to the XPS and UPS systems for characterizations. Pass energy values are 160 eV for XPS wide scan, 10 eV for high resolution scan, and 5 eV for UPS. All the data analysis about XPS and UPS was performed using the CASA XPS software. All the elements were fitted with the 70% Gaussian and 30% Lorentzian peak shapes after applying background subtractions with Shirley function.[4]

SCLC Measurement: The devices (Au/$Cs_2AgBiBr_6$singlecrystal/Au) were fabricated and used for the trap density. The dark I-V curve was measured using Keithly4200 semiconducting equipment and used to calculate the trap density. The measurements were performed at room temperature.

Photoresponsivity and Detectivity of $Cs_2AgBiBr_6$ Single-Crystalline Photodetectors. Photoresponsivity (R) and detectivity (D*) are two crucial parameters for photodetectors, where R is defined as the ratio of photocurrent to incident light intensity, which can be calculated, [5,6]

$$R = \frac{I_{ph}}{P_o S} \qquad (1),$$

where I_{ph} is the difference between the light current and dark current ($I_{ph} = I_{light} - I_{dark}$), P_0 is the irradiance power density, and S is the effective illuminated area. The unit of R is mA/W.

The corresponding detectivity (D*) of the devices can be calculated by the following equation,[7]

$$D^* = \frac{R\sqrt{A}}{\sqrt{2qI_d}} \qquad (2),$$

where q is the elementary charge.

The complete expression for the active area normalized detectivity (D*) is provided in Equation (3). It is worth noting that this formula is based on the noise current (i_n) of the devices with A as the active area, B as the electrical bandwidth, and R as responsivity. In the strict sense, the noise current of photodetectors is usually tested under the high frequency conditions so the frequency dependent parameters of 1/f noise (i.e., flicker noise) and the generation-recombination noise ($i_{g\text{-}r}$) can be taken into account in addition to the frequency independent parameters of shot noise (i_s) and thermal noise (i_t); Equation (4).

$$D^* = \frac{R\sqrt{AB}}{i_n} \qquad (3)$$

$$i_n = \sqrt{i_s^2 + i_t^2 + i_{1/f}^2 + i_{g-r}^2} \qquad (4)$$

Because the precise determination of noise current in photodetectors is challenging to test, it is a common practice to estimate i_n from the dark current and shunt resistance (R_{sh}) with the assumption that 1/f and g-r noises are negligible (see ref. 8 for more details). Therefore, i_n is often estimated by the simplified version of Equation (4) taking into account i_s and/or i_t; Equations (5) and (6).

$$i_s = \sqrt{2eI_D B} \qquad (5)$$

$$t_t = \sqrt{\frac{4KTB}{R_{sh}}} \qquad (6)$$

As discussed in the previous work by Yang and coworkers,[9] the dark current dominated by the shot noise regime was assumed and D* can be expressed by the formula: $D^* = \frac{J_{ph}/L_{light}}{\sqrt{2qJ_d}}$, where J_{ph} and J_d (= I_D/A) are the light and dark current and q is the elementary charge, L_{light} is the incident light intensity. It is worth noting that J_{ph}/L_{Light} is Responsivity, R, which leads to Equation (6). Similarly, in another paper published by Jie and coworkers,[7] they assumed that the dark current is dominated by the shot noise for estimating D* by using a formula as follows: $D^* = \frac{R\sqrt{A}}{\sqrt{2qI_d}} = \frac{R}{\sqrt{2qJ_d}}$. Following the strategy adopted in literature to calculate D*, we considered the case of $i_n \sim i_s$ (i.e., shot noise dominant regime in the dark current) and by substituting Equation (5) into Equation (3), we arrived at Equation (2) and determined the detectivity of our $Cs_2AgBiBr_6$ single crystal based photodetectors.[8, 9]

The units of D* is Jones (or cm $Hz^{1/2}$ W^{-1}).

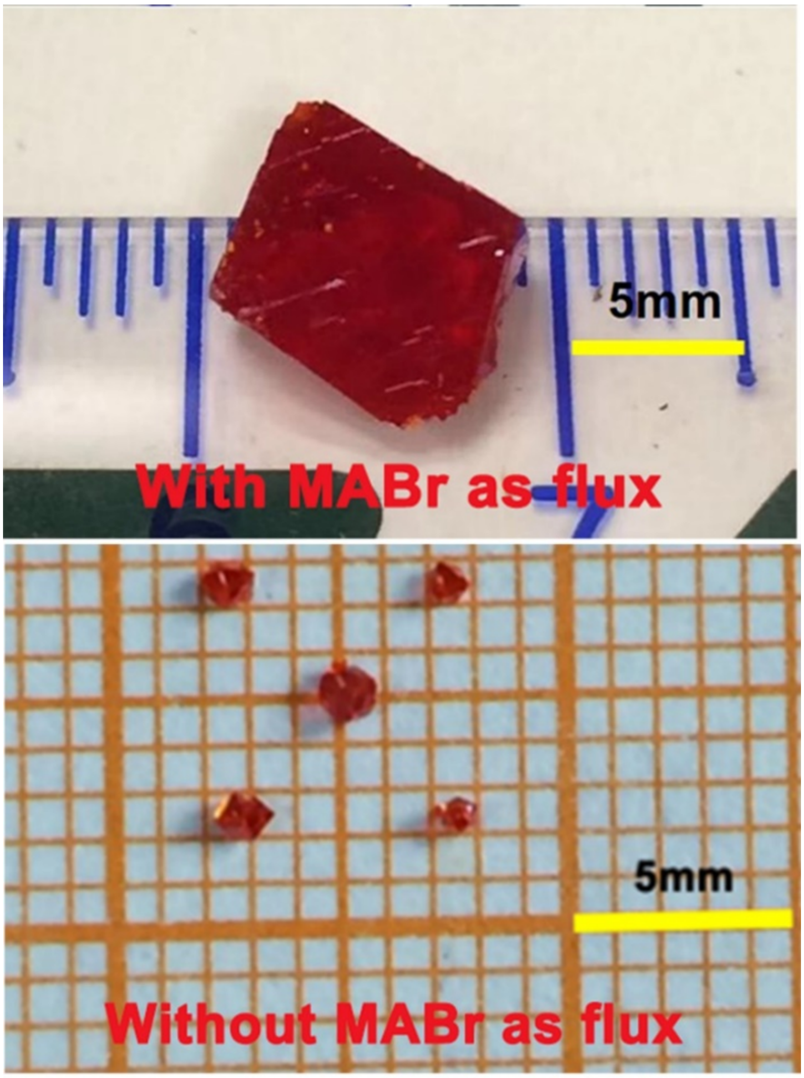

Fig. S1 Photos of $Cs_2AgBiBr_6$ single crystals with and without MABr as flux

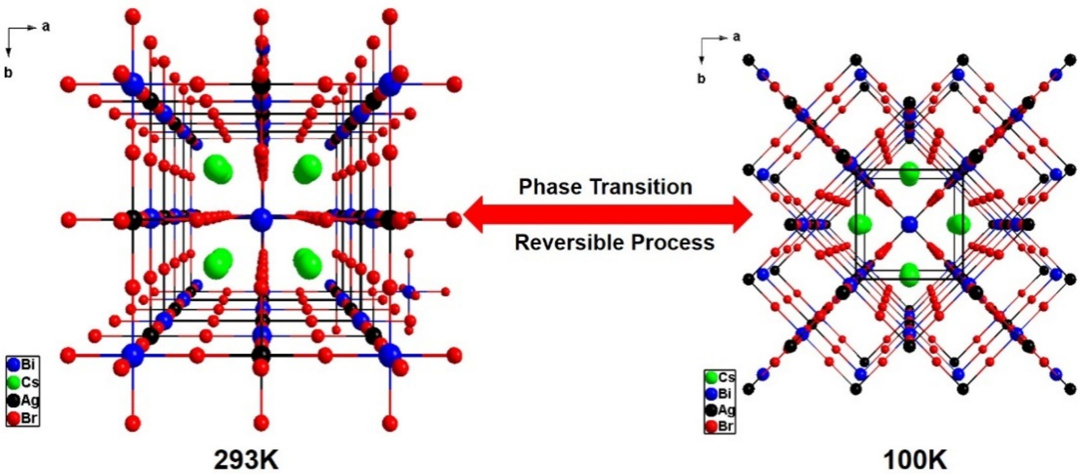

Fig. S2. Crystal structures of $Cs_2AgBiBr_6$ single crystals at 293 K and 100K

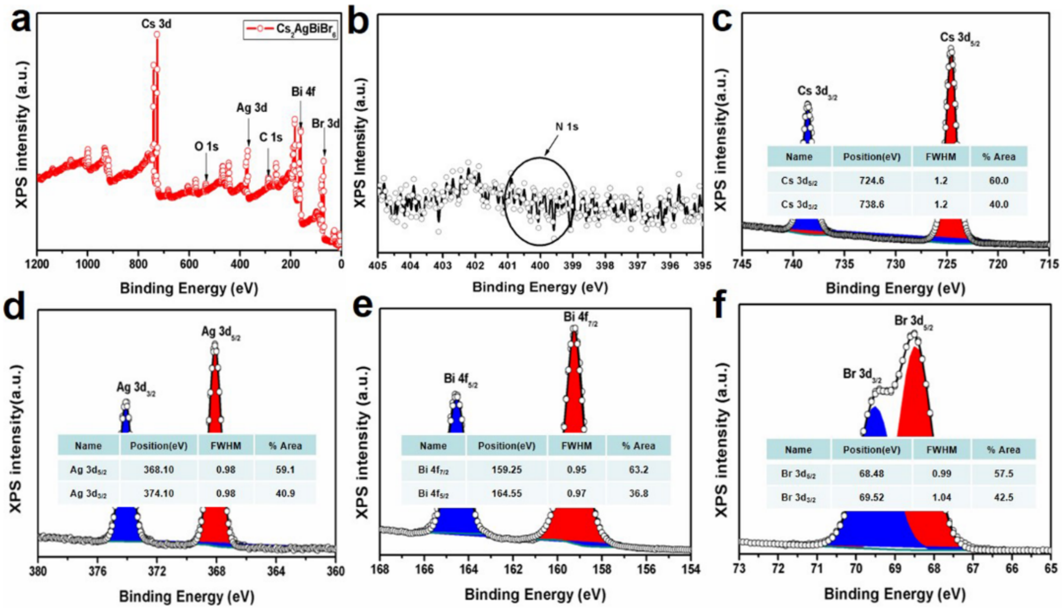

Fig. S3. Core level XPS spectra for (a) wide scan of $Cs_2AgBiBr_6$ single crystal, (b) N 1s, (c) Cs 3d, (d) Ag 3d, (e) Bi 4f and (f) Br 3d, fitted with peaks having a 70 % Gaussian and 30 % Lorentzian peak shape after applying background subtraction with Shirley function.

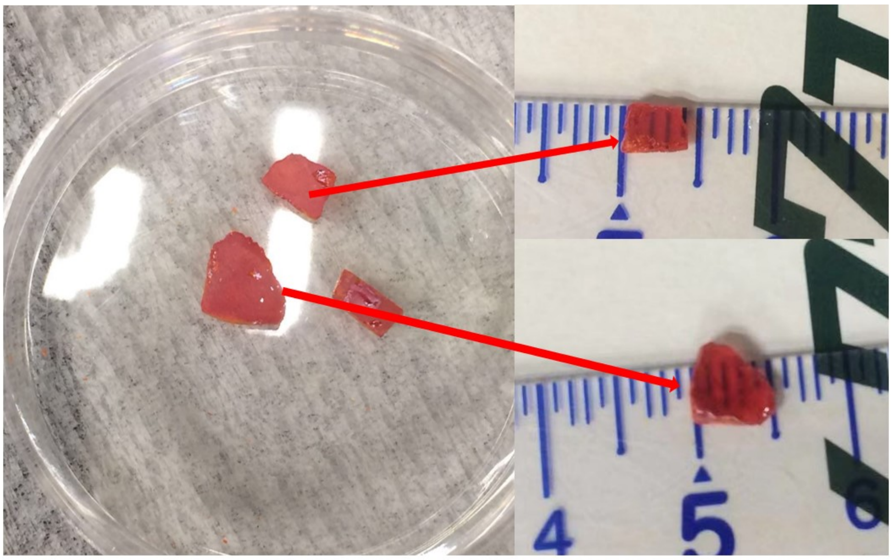

Preliminary cleaving by abrasive paper Silk cloth polishing

Fig. S4. High quality $Cs_2AgBiBr_6$ single crystal surfaces obtained by mechanical polishing using abrasive paper and then silk cloth.

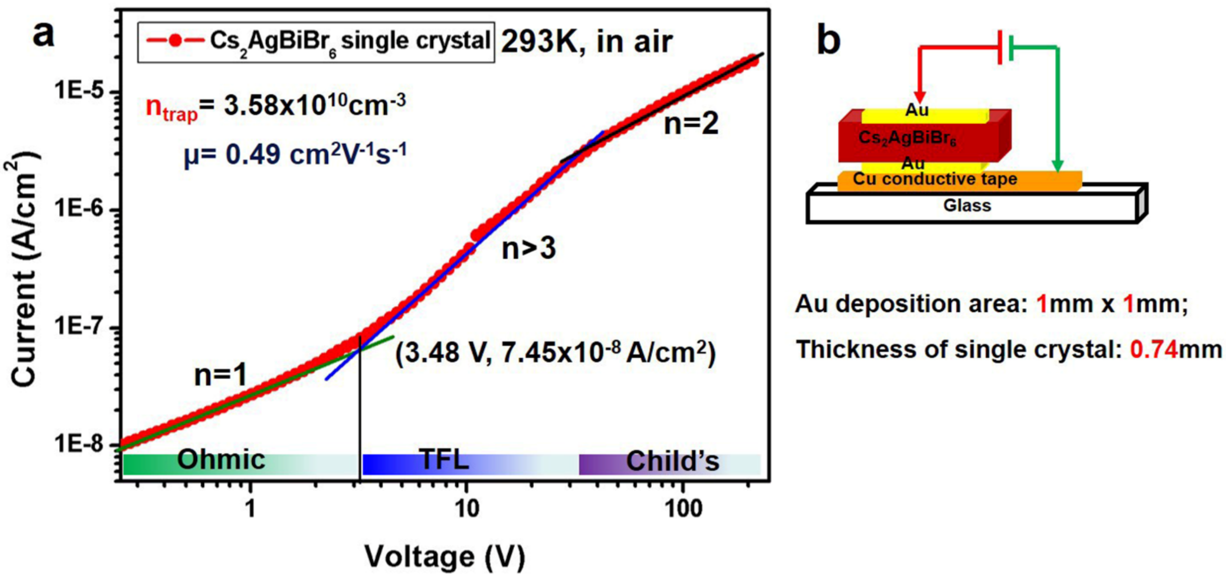

Figure S5. (a) Current-voltage measurements of the $Cs_2AgBiBr_6$ single crystal in dark. The three regions of Ohmic, trap-filling limit (TFL), and space charge limited current (SCLC) of the $Cs_2AgBiBr_6$ single crystal are delineated. The onset of TFL determines the trap density (n_{trap}), while carrier mobility (μ) is determined based on the SCLC regime. (b) Schematic illustration of the device based on $Cs_2AgBiBr_6$ single crystals sandwiched between two Au electrodes. Inset: area of the Au electrode (1 mm × 1 mm) and thickness of the single crystal (0.74 mm)

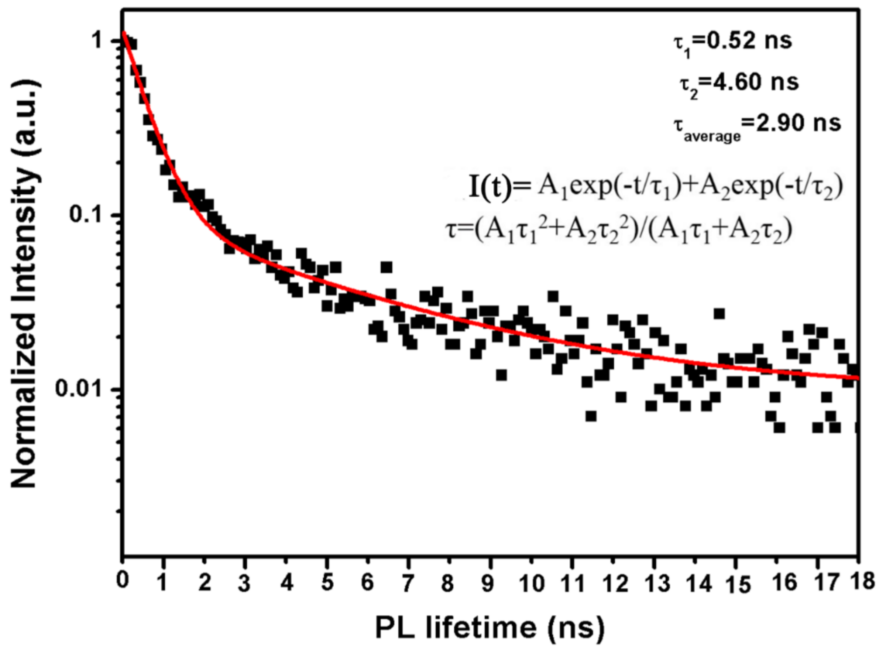

Fig. S6. PL decay lifetime of $Cs_2AgBiBr_6$ single crystals, using biexponential fitting.

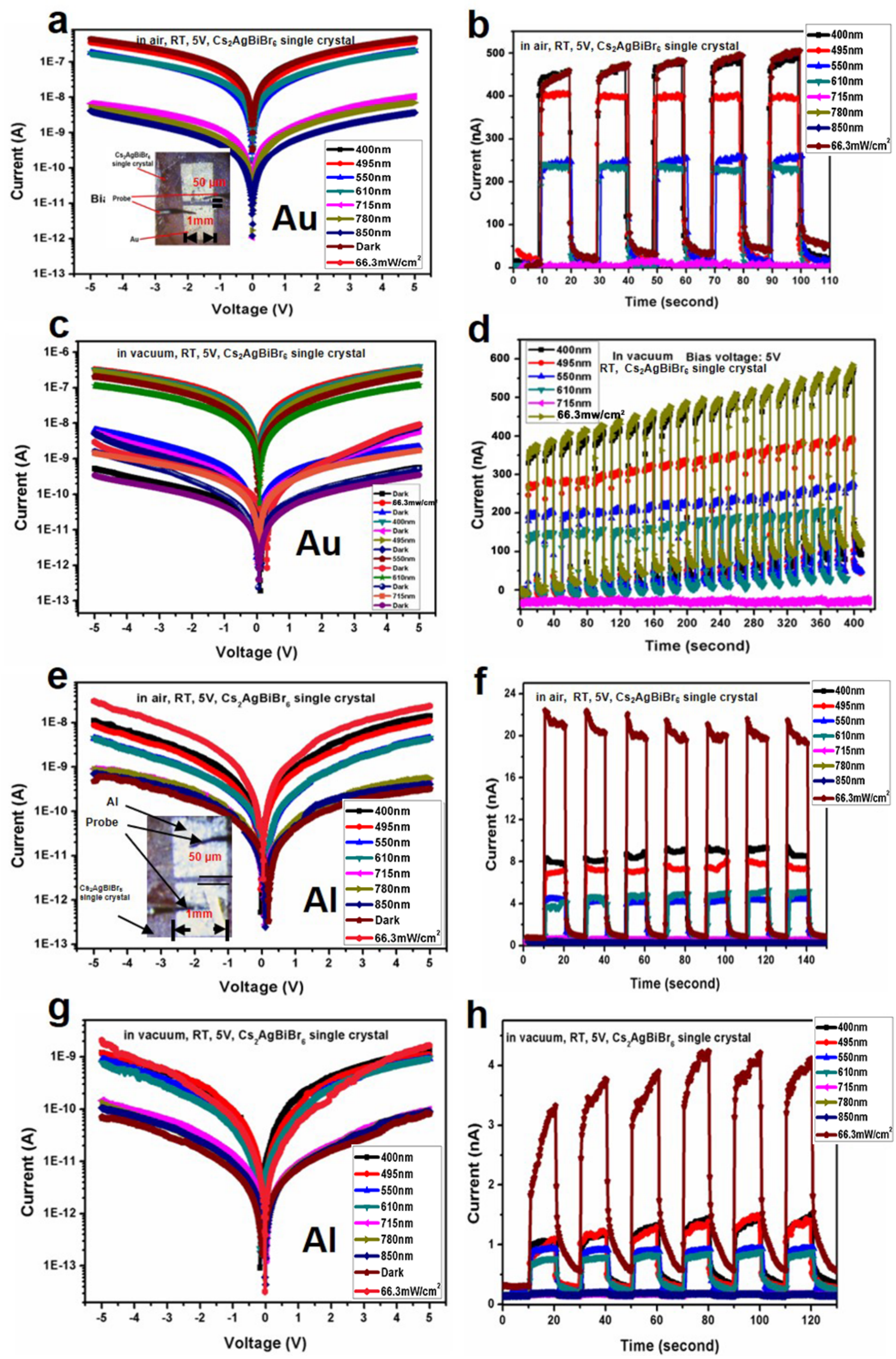

Fig. S7. (**a-d**) Photodetector data (I-V and I-time curves) of $Cs_2AgBiBr_6$ single crystal based on Au electrodes under different wavelength at room temperature when measured in air with a relative humidity of 20 % and under vacuum conditions (P = 3 × 10^{-7} Torr); (**e-h**) Photodetector data (I-V and I-time curves) of $Cs_2AgBiBr_6$ single crystal based on Al electrodes under different wavelength at room temperature when measured in air with a relative humidity of 20% and under vacuum conditions (P = 3 $\times 10^{-7}$ Torr).

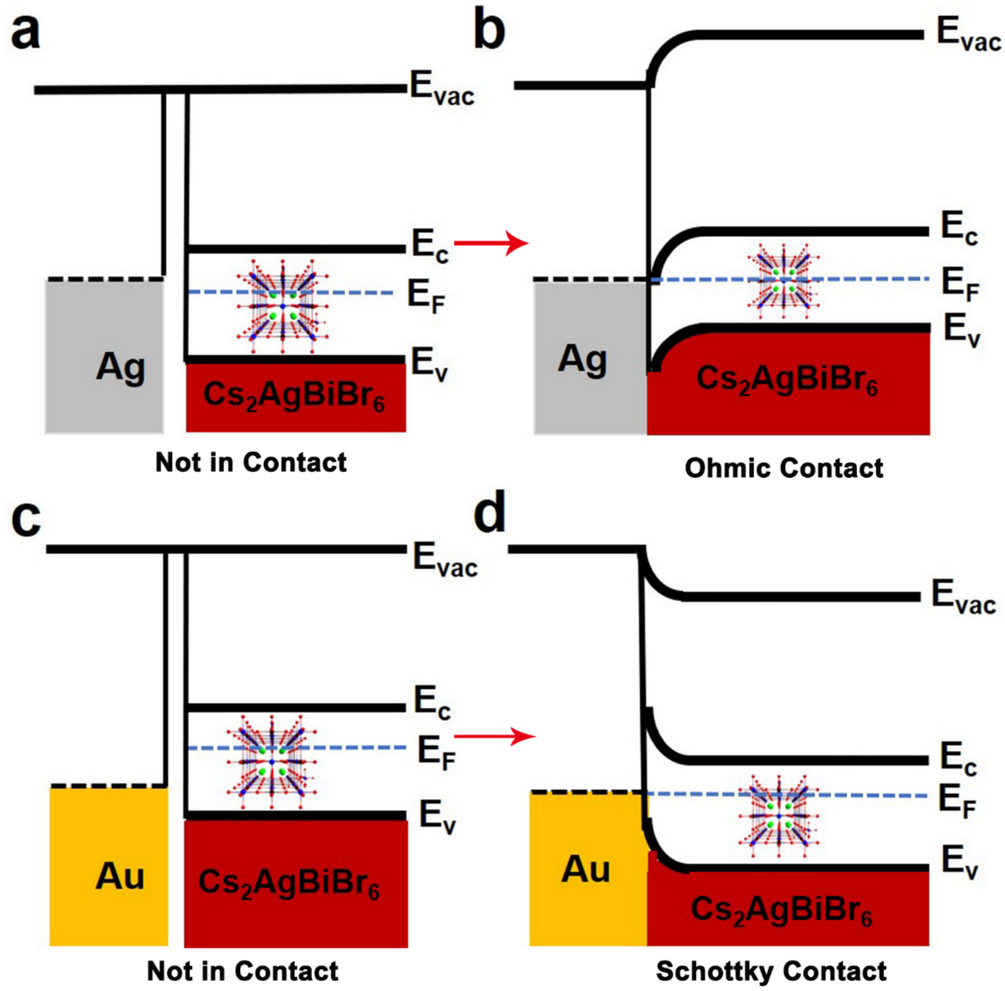

Fig. S8. Energy band diagrams of the $Cs_2AgBiBr_6$ single-crystalline devices using different electrodes not in contact and in contact in the dark condition. Energy band diagrams of the $Cs_2AgBiBr_6$ single-crystalline devices using Ag electrodes not in contact (**a**) and in contact (**b**) in the dark condition; Energy band diagrams of the $Cs_2AgBiBr_6$ single-crystalline devices using Au electrodes not in contact (**c**) and in contact (**d**) in the dark condition.

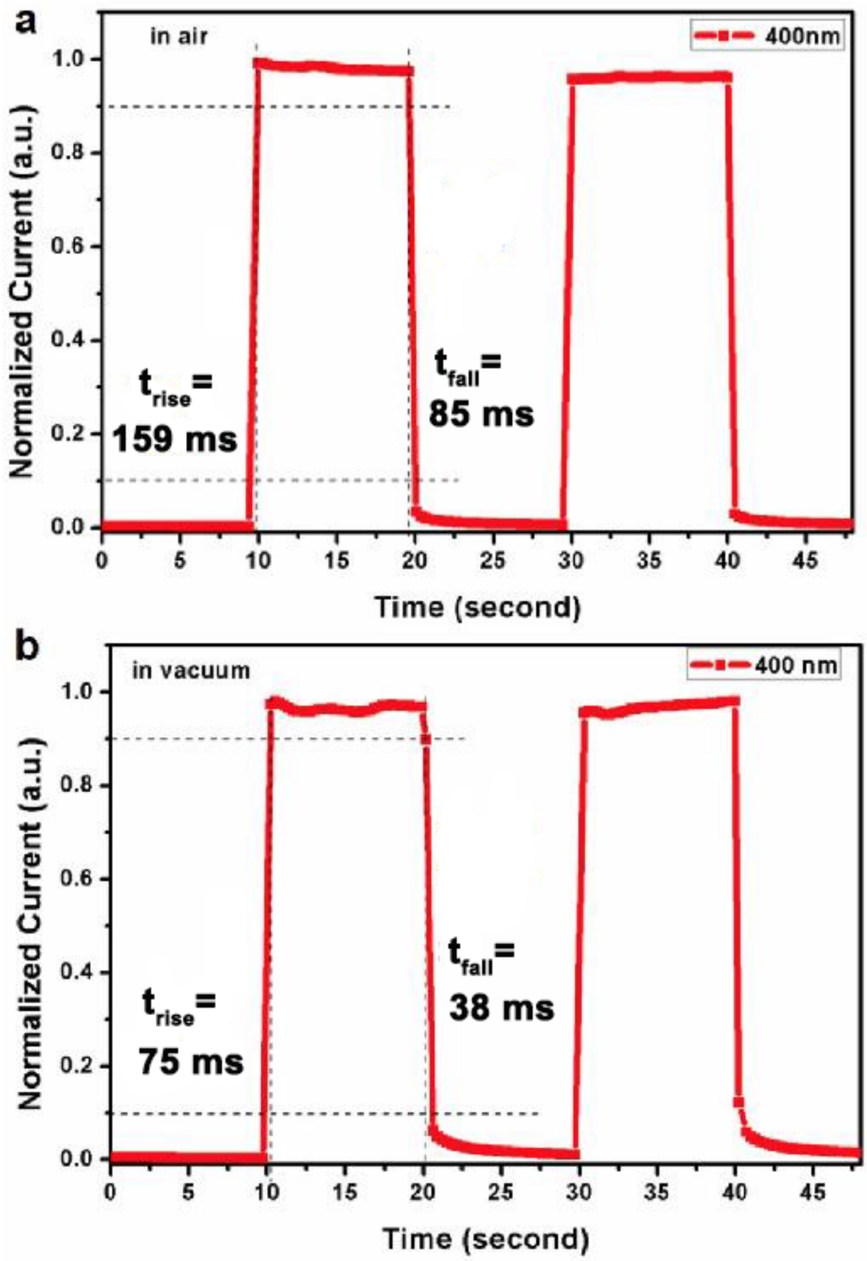

Fig. S9. Response time and decay time of $Cs_2AgBiBr_6$ single-crystalline photodetectors. (a) Response times of rise time (t_{rise} = 159 ms) and decay time (t_{fall} = 85 ms) of $Cs_2AgBiBr_6$ single-crystalline photodetectors in air atmosphere; (b) Response times of t_{rise} = 75 ms and t_{fall} =38 ms of $Cs_2AgBiBr_6$ single-crystalline photodetectors in vacuum.

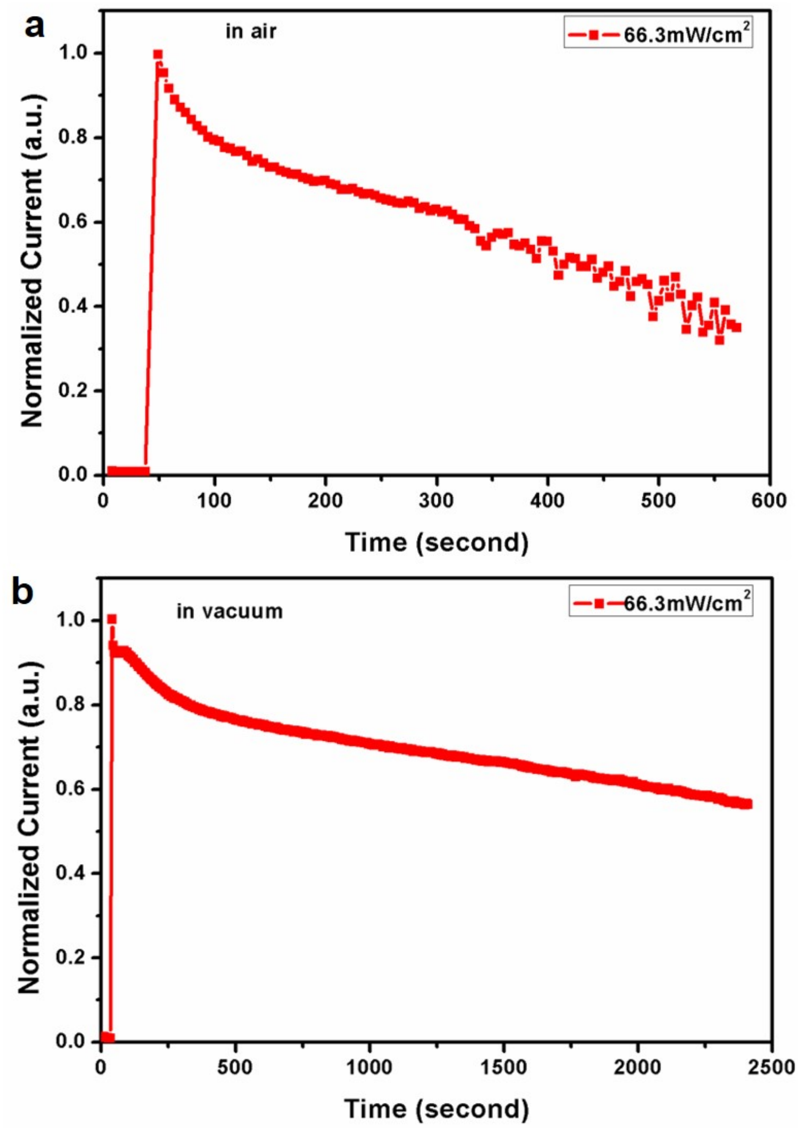

Fig. S10. Stability of $Cs_2AgBiBr_6$ single-crystalline photodetectors in air and vacuum atmosphere at room temperature.

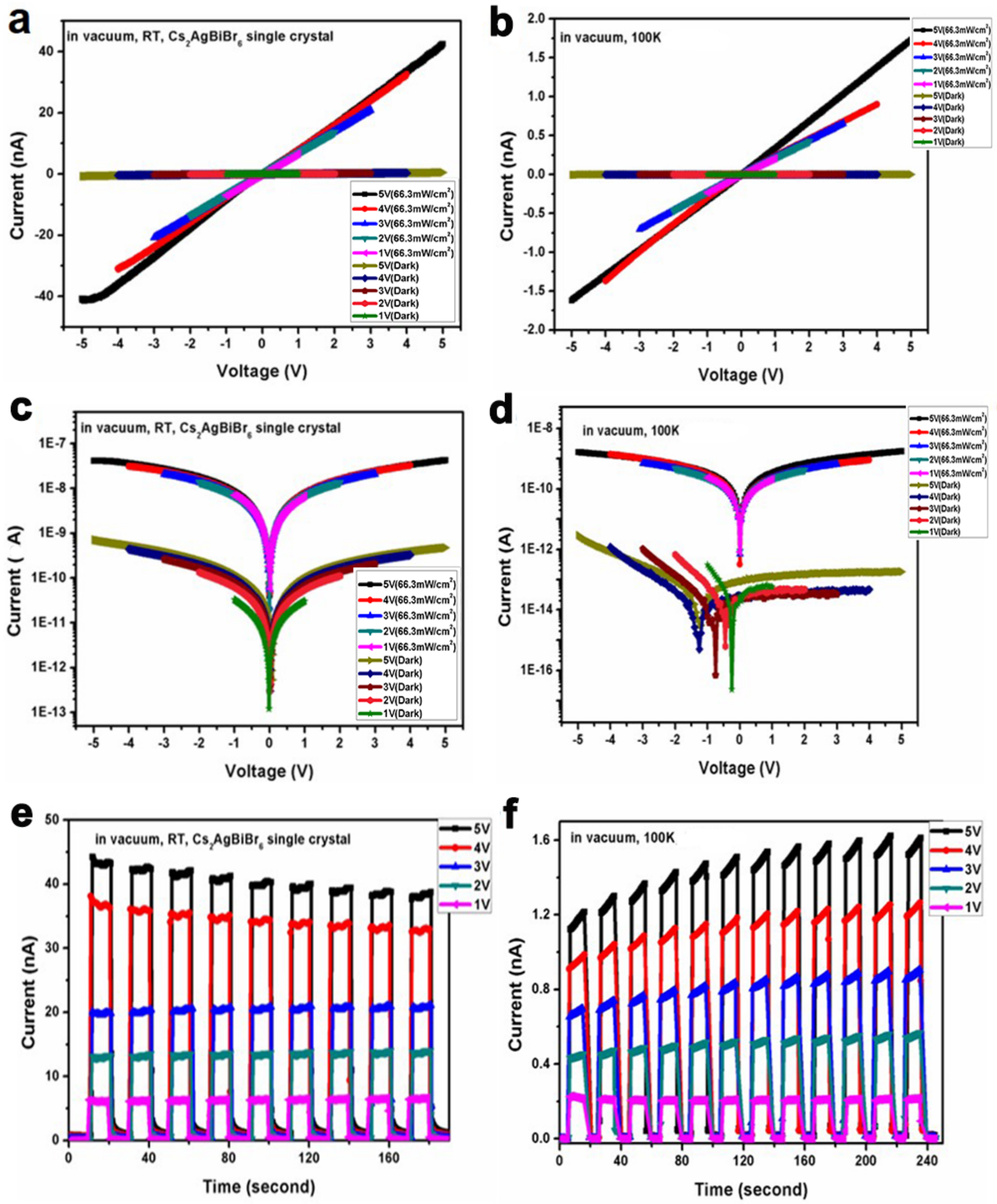

Fig. S11. (**a, c, e**) Photodetector data (I-V and I-time curves) of $Cs_2AgBiBr_6$ single crystal based on Ag electrodes at room temperature (293K); (**b, d, f**) Photodetector data (I-V and I-time curves) of $Cs_2AgBiBr_6$ single crystal based on Ag electrodes at low temperature (100K). All the measurements were performed under vacuum conditions (P = 3x10^{-7} Torr).

Table S1. Crystal data and structure refinements for $Cs_2AgBiBr_6$ at 293 K and 100 K

Empirical formula	$Cs_2AgBiBr_6$ ^{a}	$Cs_4Ag_2Bi_2Br_{12}$ ^{b}	$Cs_4Ag_2Bi_2Br_{12}$ ^{c}
Formula weight/ g·mol^{-1}	1062.13	2124.26	2124.26
Temperature/K	100 K		293 K
Wavelength/Å	0.71073		
Crystal color	yellow	yellow	red
Crystal system	tetragonal	cubic	cubic
Space group	*I*4/m (no. 87)	*F*m-3m (no. 225)	*F*m-3m (no. 225)
a/Å	7.8943(4)	11.1982(10)	11.2528(11)
b/Å	7.8943(4)	11.1982(10)	11.2528(11)
c/Å	11.2420(11)	11.1982(10)	11.2528(11)
α/°	90.00	90.00	90.00
β/°	90.00	90.00	90.00
γ/°	90.00	90.00	90.00
Volume/Å^3	700.60(10)	1404.3(4)	1424.9(4)
Crystal size (mm^3)	0.2×0.15×0.1	0.2×0.15×0.1	0.15×0.12×0.1
Z	2	2	2
Density/g·cm^{-3}	5.035	5.024	4.951
μ(mm^{-1})	36.118	36.039	35.517
F (000)	900	1800	1800
GOF on F^2	1.292	1.505	1.160
Absorption correction	Semi-empirical from equivalents		
Refinement method	Full-matrix least-squares on F^2		
Data/restraints/parameters	434/0/17	113/0/8	115/0/8
R_1, wR_2 [I > 2σ (I)]	0.0684, 0.1620	0.0516, 0.1202	0.0118, 0.0288
R_1, wR_2 (all data)	0.0684, 0.1620	0.0516, 0.1202	0.0118, 0.0288
Max / MinΔρ /eÅ^{-3}	9.98/-8.70	7.78/-5.73	0.68/-0.73
CCDC	1919712	1919713	1919714

$^{a}w=1/[s^2(Fo^2)+(0.000P)^2+212.7582P]$ where $P=(Fo^2+2Fc^2)/3$

$^{b}w=1/[s^2(Fo^2)+(0.000P)^2+498.1188P]$ where $P=(Fo^2+2Fc^2)/3$

$^{c}w=1/[s^2(Fo^2)+(0.0100P)^2+4.5254P]$ where $P=(Fo^2+2Fc^2)/3$

Table S2. Device parameters for $Cs_2AgBiBr_6$ single-crystalline photodetectors using Ag electrodes at different condition at 293 K

Device	Condition	Dark current	Light current	R (mA/W)	D* (Jones)	On/off
Ag electrode	400 nm in air (293 K)	$6.83x10^{-10}$ A	$2.88x10^{-8}$ A	0.90	$1.38x10^{9}$	42
	400 nm in vacuum (293 K)	$1.86x10^{-10}$ A	$2.86x10^{-8}$ A	0.92	$2.66x10^{9}$	153

Table S3. Comparison of perovskite single crystal photodetectors in this work and previous reports operated in ambient air condition.

Material	Wavelength	Voltage	R	D*	Response time	ON/OFF	Ref
$Cs_2AgBiBr_6$ SC	400 nm	5V	0.9 mA W^{-1}	~10^{9} Jones	159/85 ms	42	This work
$CH_3NH_3PbI_3$ SC	white light	4 V	7.92 A W^{-1}	_	0.2/0.2 s	_	10
$CsPbBr_3$ SC	442 nm	5 V	2 A W^{-1}	_	69/261 μs	10^{3}	11
$CsPbBr_3$ SC	550 nm	0 V	28 mA W^{-1}	~10^{11} Jones	230/60 ms	10^{5}	12
$CsPbBr_3$ SC	450 nm	5 V	28 mA W^{-1}	~10^{11} Jones	100/100 ms	10^{2}	13
$Cs_2AgInCl_6$ SC	365 nm	5 V	13 mA W^{-1}	~10^{12} Jones	0.97 ms	_	14
$(TMHD)BiBr_5$	Less 600 nm	10 V	0.1 A W^{-1}	_	9.6/10.3 ms	10^{3}	15
$Cs_2AgBiBr_6$ thin films	510 nm	5 V	-	-	-	7	16

References

1 O. V. Dolomanov, L. J. Bourhis, R. J. Gildea, J. A. K. Howard, H. Puschmann, *J. Appl. Cryst.* 2009, **42,** 339.

2 G. M. Sheldrick, *Acta Cryst.*2008, **A64,** 112.

3 W. M.Wendlandt, H. G. Hecht, *Reflectance Spectroscopy*; Interscience: New York, 1966; p62.

4 W. Song, K. Leung, Q. Shao, K. J. Gaskell, J. E. Reutt-Robey, *J. Phys. Chem. C* 2016, **120,** 22979.

5 L. Liang, P. C. Wu, X. S. Fang, T. Y. Zhai, L. Dai, M. Y. Liao, Y. Koide, H. Q. Wang, Y. Bando, D. Golberg, *Adv. Mater.* 2010, **22,** 3161.

6 J. S. Miao, W. D. Hu, N. Gao, Z. Y. Lu, X. Q. Liu, L. Liao, P. P. Chen, T. Jiang, S. W. Wu, J. C. Ho, L. Wang, X. S. Chen, W. Lu, *Small* 2015, **11**, 936.

7 J. Mao, Y. Q. Yu, L. Wang, X. J. Zhang, Y. M. Wang, Z. B. Shao, J. S. Jie, *Adv. Sci.* 2016, **3**, 1600018.

8 J. Miao,F. Zhang, *Laser Photonics Rev*. 2019, **13**, 1800204

9 (a) G. Tong, X. Geng, Y. Yu, L. Yu, J. Xua, Y. Jiang, Y. Sheng, Y. Shi and K. Chen, *RSC Adv*., 2017, **7**, 18224; (b) L. Dou, Y. M. Yang, J. You, Z. Hong. W. H. Chang, G. Li, and Y. Yang, *Nat. Commun.*, 2014, **5**, 5404; (c) S. Gu,K. Ding, J. Pan, Z. Shao, J. Mao, X. Zhang and J. Jie, *J. Mater. Chem. A*, 2017, **5**, 11171.

10 H. Fang, Q. Li, J. Ding, N. Li, H. Tian, L. Zhang, T. Ren, J. Dai, L. Wang, Q. Yan, *J. Mater. Chem. C* 2016, **4**, 630.

11 J. Song, Q. Cui, J. Li, J. Xu, Y. Wang, L. Xu, J. Xue, Y. Dong, T. Tian, H. Sun, H. Zeng, *Adv. Opt. Mater*. 2017, **5**, 1700157.

12 M. I. Saidaminov, M. A. Haque, J. Almutlaq, S. Sarmah, X.-H. Miao, R. Begum, A. A. Zhumekenov, I. Dursun, N. Cho, B. Murali, O. F. Mohammed, T. Wu, O. M. Bakr, *Adv. Opt. Mater.* 2017, **5**, 1600704.

13 J. Ding, S. Du, Z. Zuo, Y. Zhao, H. Cui, X. Zhan, *J. Phys. Chem. C* 2017, **121**, 4917.

14 J. Luo, S. Li, H. Wu, Y. Zhou, Y. Li, J. Liu, J. Li, K. Li, F. Yi, G. Niu, J. Tang, *ACS Photonics* 2018, **5**, 398.

15 C. Ji, P. Wang, Z. Wu, Z. Sun, L. Li, J. Zhang, W. Hu, M. Hong, J. Luo, *Adv. Funct. Mater.* 2018, **28**, 1705467.

16 J. Xiu, Y. Shao, L. Chen, Y. Feng, J. Dai, X. Zhang, Y. Lin, Y. Zhu, Z. Wu, Y. Zheng, H. Pan, C. Liu, X. Shi, X. Cheng, Z. He, *Mater. Today Energy* 2019, **12**, 186.